CERN-TH/2001-036
IPPP/01/62
DCPT/01/24
December 24, 2001

A study of single sneutrino production at polarised photon colliders

Dilip Kumar Ghosh[a,1] **and Stefano Moretti**[b,2]

[a] *Department of Physics, National Taiwan University*
Taipei, TAIWAN 10617, Republic of China

[b] *CERN Theory Division, CH-1211 Geneva 23, Switzerland*
and
Institute for Particle Physics Phenomenology, University of Durham, Durham DH1 3LE, UK

Abstract

We investigate single sneutrino production in the context of R-parity-violating Supersymmetry at future $\gamma\gamma$ linear colliders. The sneutrino is produced in association with fermion pairs and it is shown that its decays into two further fermions will lead to a clean signal. We also discuss possible backgrounds and the effects of beam polarisation.

PACS Nos.: 12.60.Jv, 13.10.+q, 14.80.Ly

[1] dghosh@phys.ntu.edu.tw
[2] Stefano.Moretti@cern.ch

1 Introduction

Supersymmetry (SUSY) is currently the most attractive theoretical framework describing physics beyond the Standard Model (SM). Even the minimal extension of the SM incorporating SUSY (MSSM) predicts a zoo of new particles, which have not yet been observed. One of the major areas of activity in high energy physics today and in the near future is to prove their existence. If SUSY is realised at the electroweak (EW) scale, many of the superparticles should be discovered at next generation hadron colliders, such as Tevatron (Run II, $\sqrt{s_{p\bar{p}}} = 2$ TeV) at FNAL and the Large Hadron Collider (LHC, $\sqrt{s_{pp}} = 14$ TeV) at CERN. These machines, while having the chance of being the first to access the SUSY domain, are however hampered by the fact that a large QCD background and the lack of knowledge of the initial centre-of-mass (CM) partonic energies render difficult the task of determining sparticle properties (masses, couplings, quantum numbers, etc.). An insight into this 'SUSY spectrum' would in fact shed light on the yet unknown mechanism leading to SUSY-breaking.

In contrast, in e^+e^- collisions, the QCD noise is under control and the initial energies of the leptons are generally well known. This has contributed in the recent years to the generation of a strong consensus behind the option of building electron-positron Linear Colliders (LCs), operating in the energy range from 500 GeV to 3 TeV, as the accelerators most suited to inherit the legacy of the Run II and LHC era [1]. Such machines would not only provide the ideal environment for discovering the SUSY particles which could be missed out at the FNAL and CERN experiments, but would also allow for the precise determination of the mentioned SUSY spectrum. For example, mass measurements are aided by the ability to perform threshold scans by varying the collider CM energy. Furthermore, the spin properties of many SUSY particles can be accessed by exploiting an efficient beam polarisation, a feature altogether missing at the Tevatron and the LHC.

Another advantage of LCs is that they can easily be converted to run quite simply in e^-e^- mode or even in $e\gamma$ and $\gamma\gamma$, the latter by using Compton back-scattering of laser photons against the electrons/positrons [2, 3], all such collisions taking place with energy and luminosity comparable to those obtainable from the primary e^+e^- design. Quite apart from SUSY [4], it should be recalled that electron-electron collisions would constitute a privileged window on, *e.g.*, models with extended Higgs sectors whereas those employing photon beams would easily allow for, *e.g.*, the study of a plethora of QCD topics.

To come back to SUSY, it should be mentioned that there have been in the recent years quite promising explorations of the physics potential of $\gamma\gamma$ LCs as a probe of the low energy dynamics of the theory [5]. It is the intention of our study to further dwell on this topic, by considering the scope of LCs in accessing some R-parity-violating (RPV) signals of SUSY.

2 R-parity-violating Supersymmetry

The construction of the most general Supersymmetric extension of the SM leads to Baryon-(B)- and Lepton-(L)-number-violating operators in the superpotential

$$W_{\not R} = \epsilon_i \lambda_{ijk} \hat{L}_i \hat{L}_j \hat{E}^c_k + \lambda'_{ijk} \hat{L}_i \hat{Q}_j \hat{D}^c_k + \epsilon_i \hat{L}_i \hat{H}_2 + \lambda''_{ijk} \hat{U}^c_i \hat{D}^c_j \hat{D}^c_k. \tag{1}$$

Here, $\hat{H}_1$, $\hat{H}_2$ are the $SU(2)$ doublets Higgs superfields which give rise to the masses of down-type and up-type quark superfields, respectively, $\hat{L}(\hat{Q})$ denotes lepton(quark) doublet superfields, $\hat{E}^c$, $\hat{D}^c$, $\hat{U}^c$ are the singlet lepton and quark superfields, i, j, k are the generational indices and we have suppressed the $SU(2)$ and $SU(3)$ indices. The λ_{ijk} are anti-symmetric in i and j while the λ''_{ijk} are anti-symmetric in j and k. The first three terms in $W_{\not R}$ violate lepton number and the last term violates baryon number conservation. The simultaneous presence of both B- and L-violating operators would induce rapid proton decay which would contradict the strict experimental bound of [6]. In order to keep the proton lifetime within the experimental limit, one needs to impose an additional symmetry beyond the SM gauge symmetry, in order to force the unwanted B- and L-violating interactions to vanish. In most cases, this can be achieved by imposing a discrete symmetry, called R-parity [7], defined as $\mathrm{R} = (-1)^{3\mathrm{B}+\mathrm{L}+2\mathrm{S}}$, where S is the spin. This symmetry not only forbids rapid proton decay [8] but also renders stable the lightest supersymmetric particle (LSP).

However, R-parity is quite an *ad hoc* assumption in nature, as there are no strong theoretical arguments to support it. Therefore, it is much justified to investigate the phenomenological consequences of RPV SUSY. Extensive studies have been carried out in order to look for direct as well as indirect evidence of trilinear R-parity violation in different processes at various colliders as well as in order to put constraints on various RPV couplings [9]. In this article, we will consider RPV single production of sneutrinos in association with fermion pairs in polarised photon-photon collisions at 500 GeV and 1 TeV LCs, and their subsequent decays into two further fermions, via trilinear L-violating operators, while preserving B-conservation. Schematically, one has

$$\gamma\gamma \to \tilde{\nu}\ell^{\pm}\ell'^{\mp} \quad \text{or} \quad \tilde{\nu}q\bar{q}' \tag{2}$$

with

$$\tilde{\nu} \to \ell''^{\pm}\ell'''^{\mp} \quad \text{or} \quad \tilde{\nu} \to q''\bar{q}''', \tag{3}$$

where the ℓ's refer to e, μ and τ leptons and the q's to d, u, s, c and b quarks.

This process has been computed recently in [10], by assuming unpolarised photon beams and without any detailed background estimates. We will improve on that study by exploiting polarised $\gamma\gamma$ scatterings, as it has been shown that a high degree of polarisation can be transmitted from the electrons, positrons and laser photons to the Compton back-scattered photons, and by including

a study of the irreducible SM background[1]. In fact, it will be shown that polarisation may help to improve the signal-to-background ratio (S/B) in some instances. We consider a general MSSM parameter space, with no assumption on the mechanism of SUSY-breaking, hence defining all parameters at the EW scale.

Before proceeding to the analysis, it is is useful to note at this point that the ϵ_i terms in (1) can in principle be removed by a re-definition of the lepton doublets $\hat{L}_i$, which would in turn lead to their 'absorption' into the λ, λ' couplings and in the parameters of the scalar potential of the SUSY model. However, the ϵ_i's could then re-appear at a different energy scale. Bilinear terms could also lead to a possible vacuum expectation value (VEV) for the sneutrino(s) and mixing of: (a) charged leptons with charginos, (b) sleptons with charged Higgs bosons, (c) neutrinos with neutralinos and (d) sneutrinos with neutral Higgs bosons. This last mixing could indeed affect the process discussed here. However, this phenomenon is suppressed by the small Yukawa couplings of our ℓ and q fermions, so that we feel justified in neglecting it here (*i.e.*, we are making the assumption that the ϵ_i terms are small)[2].

The paper is organised as follows. In section 3, we discuss the phenomenology of processes (2)–(3) in presence of polarised incoming photons. In section 4 we present our numerical results (including those for the backgrounds), followed by our conclusions in section 5.

3 Singly produced sneutrinos at polarised photon colliders

In the RPV MSSM, the sneutrino displays a coupling with pairs of leptons (λ-type couplings) and quarks (λ'-type couplings). Single production of sneutrino in association with fermion pairs in (2) can occur through any of these two types of L-violating couplings. Depending upon the nature of the vertex involved, the above process may also lead to flavour changing final states.

The polarised photon flux and polarisation have been worked out in [2] and are discussed in details in Ref. [3]. For brevity, we do not reproduce here those formulae, rather we simply recall to the un-familiar reader the basic features of polarised $\gamma\gamma$ scatterings.

1. We assume that the laser back-scattering parameter assumes its maximum value, $z \equiv z_{\rm max} = 2(1+\sqrt{2}) \simeq 4.828$ [2]. In fact, with increasing z the high energy photon spectrum becomes

[1] We make use of HELAS [11] and MadGraph [12] to produce the helicity amplitudes, for both signal and backgrounds, and integrate these numerically by using VEGAS [13].

[2] This would not be possible for processes involving top (anti)quarks, because of their large mass. However, in (2)–(3), t quarks contributions will have negligible impact, because strongly suppressed by phase space effects. (Some phenomenological consequences of a sneutrino VEV and L-violating mixing have been discussed in literature [14].)

more mono-chromatic. However, for $z > z_{\max}$, the probability of e^+e^- pair creation increases, resulting in larger photon beam degradation.

2. The reflected photon beam carries off only a fraction x of the $e^\pm$ energy, with $x_{\max} = z/(1+z) \simeq 0.8$, while $x_{\min} = (M_{\tilde{\nu}} + m_f + m_{\bar{f}'})/\sqrt{s_{e^+e^-}}$ (hereafter, $f^{(')} = \ell, q$).

3. The polarization of the two initial laser (γ) and electron/positron (e) beams are defined by $P_{\gamma_-}, P_{\gamma_+}, P_{e^-}$ and P_{e^+}, respectively, where, for the first two quantities, $-(+)$ identifies the laser colliding against the electron(positron).

4. Finally, one can cast the polarised production cross-section in the following form:

$$\begin{aligned}\sigma_{e^+e^-\to\gamma\gamma\to\tilde{\nu}f\bar{f}'}(s) = & \int dx_- dx_+ F_-^{\gamma/e}(P_{e^-}, P_{\gamma_-}, x_-; P_-) F_+^{\gamma/e}(P_{e^+}, P_{\gamma_+}, x_+; P_+) \\ & \times \hat{\sigma}_{\gamma\gamma\to\tilde{\nu}f\bar{f}'}(\hat{s}, P_-, P_+), \end{aligned} \tag{4}$$

where $x_{-(+)}$ is the electron(positron) momentum fraction carried by the emerging photon, $x_-x_+ = \hat{s}_{\gamma\gamma}/s_{e^+e^-}$, with $s_{e^+e^-}(\hat{s}_{\gamma\gamma})$ being the CM energy squared of the $e^+e^-(\gamma\gamma)$ system, and $F_\pm^{\gamma/e}(P_{e^\pm}, P_{\gamma_\pm}, x_\pm; P_\pm)$ the photon distribution functions, defined in terms of $P_{e^\pm}, P_{\gamma_\pm}$ and $x_\pm$ and yielding $P_-(P_+)$, the degree of polarisation of the photon that has back-scattered against the electron(positron)[3]. Therefore, in terms of helicity amplitudes one has (here, for brevity, $\hat{\sigma} \equiv \hat{\sigma}_{\gamma\gamma\to\tilde{\nu}f\bar{f}'}$)

$$\begin{aligned}\hat{\sigma}(\hat{s}, P_-, P_+) = & \frac{1}{4} [(1+P_-)(1+P_+)\hat{\sigma}_{++}(\hat{s}) + (1+P_-)(1-P_+)\hat{\sigma}_{+-}(\hat{s}) \\ & + (1-P_-)(1+P_+)\hat{\sigma}_{-+}(\hat{s}) + (1-P_-)(1-P_+)\hat{\sigma}_{--}(\hat{s})]. \end{aligned} \tag{5}$$

As polarised γ-structure functions we have used those of Ref. [15].

The flavour of the final state fermions will depend upon the RPV couplings involved. It has been shown that most of the first two generation L-violating terms are highly constrained from different low and medium energy processes [16]. For our study, we made the assumption that just one L-violating coupling at a time is the dominant one, so that only bounds derived under the same hypothesis are relevant. This restriction may seem unnatural, however, it is a useful approach that allows one to derive a quantitative feeling for the phenomenological consequences of RPV interactions, while avoiding a proliferation of SUSY input parameters. In our analysis, we will concentrate on the following L-violating couplings: $\lambda_{311}, \lambda_{323}, \lambda'_{323}$ and λ'_{333}. The reason for selecting this particular set out of the 36 possible couplings is that these are less constrained and at the same time can lead to a significant contribution to the production as well as the decay rates of sneutrinos in (2)–(3). The upper limits on these couplings are shown in Table 1.

[3]Conventionally, one has $P_{-(+)} = -1(+1)$ for purely left(right) handed photons.

Coupling	Upper Limit
λ_{311}	0.062
λ_{323}	0.070
λ'_{323}	0.52
λ'_{333}	0.45

Table 1: Experimental upper bounds on the RPV couplings relevant to this analysis. All sfermion masses are assumed to be ≈ 100 GeV.

Once the sneutrino is produced, it will decay. Depending on its nature, the dominant decay modes are:

$$\tilde{\nu} \;\to\; f\bar{f}' \quad (f=\ell,q) \quad \text{fermion pairs}, \tag{6}$$

$$\tilde{\nu} \;\to\; \tilde{\chi}_i^0\nu \;\; (i=1,2,3,4) \;\; \text{neutralino} \;+\; \text{neutrino}, \tag{7}$$

$$\tilde{\nu} \;\to\; \tilde{\chi}_i^+\ell^- \;\; (i=1,2) \;\; \text{chargino} \;+\; \text{lepton}. \tag{8}$$

If the sneutrino is the LSP, then it will decay through the first (RPV) channel, otherwise via one of the other two (MSSM) modes. We show the sneutrino branching ratio (BR) into two fermion final states in the $\mu - M_2$ plane for a fixed value of $\tan\beta$, RPV coupling and sneutrino mass. In the course of the analysis we assume the Grand Unification (GUT) relationship between the $U(1)$ and $SU(2)$ gaugino mass parameters: *i.e.*,

$$M_1 = \frac{5}{3}\tan^2\theta_W M_2. \tag{9}$$

Hence, the sneutrino BR into two fermions will depend upon $\mu, M_2, \tan\beta$, $M_{\tilde{\nu}}$ and the magnitude of the RPV coupling. To study the variation of the sneutrino RPV BR we have spanned μ from -500 GeV to $+500$ GeV and M_2 from 100 GeV to 500 GeV.

In Figure 1(a) we show the contours of constant BR($\tilde{\nu}_\tau \to e^+e^-$) through the λ_{311} coupling for $M_{\tilde{\nu}_\tau} = 100$ GeV in the $\mu - M_2$ plane, with $\tan\beta = 5$. The region labelled by 'LEP DISALLOWED' is ruled out from the kinematic limit on the lighter chargino mass extracted from LEP-2 data. It can be seen from this Figure that the mentioned BR is 90% over a large part of the parameter space. In this case, the lighter chargino is heavier than the sneutrino mass, forbidding the $\tilde{\nu} \to \tilde{\chi}_1^+\ell^-$ decay channel. The only MSSM channel allowed is $\tilde{\nu} \to \tilde{\chi}_1^0\nu$, which dominates in the low M_2 region, where $M_{\tilde{\chi}_1^0} < M_{\tilde{\nu}}$. The above scenario changes once the sneutrino becomes heavier, as shown in Figure 1(b), where the same BR as above is plotted but now with $M_{\tilde{\nu}} = 200$ GeV. In this case, both channels $\tilde{\nu} \to \tilde{\chi}_1^+\ell^-$ and $\tilde{\nu} \to \tilde{\chi}_1^0\nu$ make a significant contribution to the total decay width of the sneutrino. (The RPV BR increases with M_2 though, since the lighter chargino

and neutralino become heavier.) In Figure 1(c), this trend becomes very clear: for a 400 GeV sneutrino most of the $\mu - M_2$ plane is covered by the MSSM decays, relegating large RPV BRs to small corners of the parameter space.

This situation changes considerably when the RPV coupling is λ'_{333}. In this case, because of the larger magnitude of the latter, as compared to λ_{311}, the BR($\tilde{\nu} \to b\bar{b}$) for a 100 GeV sneutrino mass covers almost the entire $\mu - M_2$ plane analysed in this paper. Even for heavier sneutrinos (*e.g.*, 200 GeV and 400 GeV), a larger area in the $\mu - M_2$ plane is dominated by the above BR, leaving a smaller region for the MSSM decays than in the previous case: see Figures 1(d)–(f). Finally, we have noticed that this general behavior of the BRs does not change for higher values of $\tan\beta$. Also, the impact of λ_{323} and λ'_{323} RPV couplings onto the decay rates induces a pattern similar to the one discussed, so we do not reproduce the corresponding Figures here.

4 Numerical analysis

We perform our numerical analysis for three different points in the MSSM parameter space allowed by LEP-2 data. These are representative of three different natures of the lightest chargino and are defined in Table 2.

Set	μ (GeV)	M_2 (GeV)	$\tan\beta$	$M_{\tilde{\chi}_1^0}$ (GeV)	$M_{\tilde{\chi}_1^\pm}$ (GeV)	Nature of $\tilde{\chi}_1^\pm$
A	-400	150	5	76. 4	150.3	Gaugino dominated state
B	200	350	40	150.4	185.6	Mixed state
C	175	500	40	155.6	169.4	Higgsino dominated state

Table 2: Set of selected points in the MSSM parameter space with LSP and lighter chargino mass (and nature) given explicitly.

Furthermore, we select the combinations of incident laser and electron beam polarisations shown in Table 3.

The choice $P_{\gamma_\pm} P_{e^\pm} < 0$ guarantees not only good mono-chromaticity, but also a high degree of circular polarisation of the produced photons as compared to the case $P_{\gamma_\pm} P_{e^\pm} > 0$. There exists a symmetry amongst the four combinations of laser polarizations, as $(+-)$ and $(-+)$ give the same result, and so do $(++)$ and $(--)$ (see also [15]).

To mimic the finite coverage of the LC detectors, we impose the following cuts on the final

	P_{γ_+}	P_{γ_-}	P_{e^+}	P_{e^-}
$\sigma(+-)$	$+1$	-1	-0.8	$+0.9$
$\sigma(++)$	$+1$	$+1$	-0.8	-0.9
$\sigma(00)$	0	0	0	0

Table 3: Values of laser and electron(positron) beam polarisations adopted in our analysis. The $\sigma(+-)$ and $\sigma(++)$ denote the corresponding polarised production cross-sections, with $\sigma(00)$ the unpolarised one.

state particles in (2)[4]:

$$5^{\rm o} \;<\; \theta \;<\; 175^{\rm o} \quad \text{(angular cut on both leptons and jets)}, \tag{10}$$

$$E_\ell \;>\; 5 \text{ GeV} \quad \text{(energy cut on leptons)}, \tag{11}$$

$$E_j \;>\; 10 \text{ GeV} \quad \text{(energy cut on jets)}. \tag{12}$$

As already mentioned, we assume that only one between the λ and λ' couplings dominates at a time. Besides, we will treat the signatures arising from the four RPV couplings considered here, *i.e.*, $\lambda_{311}, \lambda_{323}, \lambda'_{323}$ and λ'_{333}, separately in the four subsections below. Where appropriate, all possible electromagnetic (EM) charge combinations (c.c.'s) will be included. Moreover, we assume that the EM charge of the leptons (e, μ and τ) can always be determined, unlike the case of quarks. For the latter, we will assume a benchmark 100% efficiency in tagging b flavours.

4.1 Signals from the λ_{311} coupling

Presence of this coupling leads $\tilde{\nu}_\tau$ to decay into e^+e^- pairs. Hence, the signal corresponding to this L-violating coupling is $e^+e^-e^+e^-$. In Figure 2(a) we show the variation of $\sigma(\gamma\gamma \to \tilde{\nu}_\tau e^+e^-) * \text{BR}(\tilde{\nu}_\tau \to e^+e^-)$ as a function of the $\tilde{\nu}_\tau$ mass for the MSSM set A, at $\sqrt{s_{e^+e^-}} = 500$ GeV. The effect of beam polarisation can be seen very clearly from the figure. At very low sneutrino masses (< 150–200 GeV), $\sigma(++)$, $\sigma(+-)$ and the unpolarised cross-section $\sigma(00)$ are basically the same. As the sneutrino mass rises, the above three cross-section display a hierarchy, though not dramatic, with $\sigma(+-) > \sigma(00) > \sigma(++)$, whereas, for $M_{\tilde{\nu}_\tau} \geq 0.5\sqrt{s_{e^+e^-}}$, the $\sigma(++)$ component is the one which largely dominates. A similar situation can be seen for the other two sets of MSSM parameters, namely sets B and C, in Figures 3(a) and 4(a), respectively. For $\sqrt{s_{e^+e^-}} = 1$ TeV, corresponding plots are given in Figures 5(a), 6(a) and 7(a), for the MSSM parameter sets A, B and C, respectively. At higher energies, the pattern is very similar, with the only exceptions

[4]We identify jets with the partons from which they originate.

that in this case $\sigma(00)$ is slightly larger than the other two at small sneutrino masses and the mentioned hierarchy onsets for somewhat larger values of the latter, in comparison to the lower energy collider option.

4.2 Signals from the λ_{323} coupling

Presence of this coupling gives rise to the following two types of signals: flavour conserving $\tau^+\tau^-\tau^+\tau^-$ and flavour changing $\mu^+\mu^-\tau^+\tau^-$ (and c.c.'s). The variation of $\sigma(\gamma\gamma \to \tilde{\nu}_\tau\mu^+\tau^-) * \mathrm{BR}(\tilde{\nu}_\tau \to \mu^-\tau^+)$ as a function of the sneutrino mass is shown in Figures 2(b) 3(b) and 4(b), for $\sqrt{s_{e^+e^-}} = 500$ GeV, and Figures 5(b), 6(b) and 7(b) for $\sqrt{s_{e^+e^-}} = 1$ TeV, corresponding to the MSSM parameter sets A, B and C, respectively. In this case the final state will have three different combinations of charged particles with identical rates: $\mu^+\mu^-\tau^+\tau^-$, $\mu^+\mu^+\tau^-\tau^-$ and $\mu^-\mu^-\tau^+\tau^+$. Hence, the individual channels will be 1/3 of the total cross-section shown in the Figures. The plots for the flavour conserving final states are displayed in Figures 2(c), 3(c) and 4(c), for $\sqrt{s_{e^+e^-}} = 500$ GeV, and Figures 5(c), 6(c) and 7(c), for $\sqrt{s_{e^+e^-}} = 1$ TeV.

In this case too we see that the dominant cross-section comes from $\sigma(++)$ once the $M_{\tilde{\nu}_\tau} \geq 0.5\sqrt{s_{e^+e^-}}$. However, al lower sneutrino masses, the pattern is different from the previous case. The ordering $\sigma(+-) > \sigma(00) > \sigma(++)$ in the intermediate mass regime and the convergence of the rates for all polarisation states at small $M_{\tilde{\nu}_\tau}$ values hold only for $\tau^+\tau^-\tau^+\tau^-$, not for $\mu^+\mu^-\tau^+\tau^-$ (plus c.c.s), for which the unpolarised cross sections are always largest. In this case, again, the increase in CM energy delays the onset of the highlighted cross section hierarchy, for $\tau^+\tau^-\tau^+\tau^-$ final states.

4.3 Signals from the λ'_{323} coupling

Presence of this coupling gives rise to the following three types of signals: the flavour conserving $s\bar{s}s\bar{s}$ and $b\bar{b}b\bar{b}$ plus the flavour changing $s\bar{s}b\bar{b}$ (and c.c.'s). The variation of $\sigma(\gamma\gamma \to \tilde{\nu}_\tau b\bar{s}) * \mathrm{BR}(\tilde{\nu}_\tau \to \bar{b}s)$ as a function of the sneutrino mass is shown in Figures 2(d), 3(d) and 4(d), for $\sqrt{s_{e^+e^-}} = 500$ GeV, and Figures 5(d), 6(d) and 7(d) for $\sqrt{s_{e^+e^-}} = 1$ TeV, again, in correspondence of the MSSM parameter sets A, B and C, respectively. Notice that in this case too there are three equiprobable signatures: $ss\bar{b}\bar{b}$, $s\bar{s}b\bar{b}$ and $\bar{s}\bar{s}bb$. Corresponding plots for the flavour conserving modes are displayed in Figures 2(e), 3(e) and 4(e), for $\sqrt{s_{e^+e^-}} = 500$ GeV, and Figures 5(e), 6(e) and 7(e) for $\sqrt{s_{e^+e^-}} = 1$ TeV (in correspondence of sets A,B and C).

The dependence upon the beam polarisation configuration is basically the same as the one described in the previous section, once one establishes a correspondence between the identical- and different-flavour final states in the two cases. The energy dependence does not differ much either from that in the two previous cases.

4.4 Signals from the λ'_{333} coupling

Presence of this coupling will also give rise to the signal $b\bar{b}b\bar{b}$. The numerical results for the corresponding production cross-sections are shown in Figures 2(f), 3(f) and 4(f), for $\sqrt{s_{e^+e^-}} = 500$ GeV, and Figures 5(f), 6(f) and 7(f) for $\sqrt{s_{e^+e^-}} = 1$ TeV, corresponding to the MSSM parameter sets A, B and C, respectively.

As for the beam polarisation dependence, here, one can see the usual dominance of $\sigma(++)$ whenever $M_{\tilde{\nu}_\tau} \geq 0.5\sqrt{s_{e^+e^-}}$, with the $\sigma(+-)$ component dominating in the intermediate regime. For lower masses, the energy dependence is such that at 500 GeV $\sigma(+-)$ is above $\sigma(00)$, whereas at 1 TeV things go the other way around.

4.5 Signals from $\tilde{\nu} \to \tilde{\chi}_1^+ \ell^-$

Here, we would like to comment about the signal cross-section $\sigma(\gamma\gamma \to \tilde{\nu} f \bar{f}) * \mathrm{BR}(\tilde{\nu} \to \tilde{\chi}_1^+ \ell^-)$ for two different RPV interactions, namely λ_{311} and λ'_{323}. Figures 8(a)–(c) correspond to $\sigma(\gamma\gamma \to \tilde{\nu}_\tau e^+ e^-) * \mathrm{BR}(\tilde{\nu}_\tau \to \tilde{\chi}_1^+ \tau^-)$ for $\lambda_{311} = 0.062$ whereas the variation of $\sigma(\gamma\gamma \to \tilde{\nu} s \bar{b}) * \mathrm{BR}(\tilde{\nu}_\tau \to \tilde{\chi}_1^+ \tau^-)$ with the sneutrino mass (for $\lambda'_{323} = 0.52$) is shown in Figures 8(d)–(f). Notice that Figures 8(a,d), 8(b,e) and 8(c,f) correspond to the three usual sets of MSSM parameters A, B and C, respectively. These cross-sections have been calculated for the case of a LC of 500 GeV. The pattern of the production and decay rates is here quite different from the one displayed for the case of RPV decays of the sneutrino. In fact, the overall behaviour in this channel depends on other factors. Firstly, on the relative mass difference between $\tilde{\nu}$ and $\tilde{\chi}_1^+$, as well as upon the composition of χ_1^+. Secondly, if it is Higgsino dominated, then the $\tilde{\nu} - \tilde{\chi}_1^+ - \ell^-$ coupling will be Yukawa suppressed. Thirdly, and most important of all, the magnitude of the RPV coupling involved: as it is clear from comparing Figures 8(a)–(c) to Figure 8(d)–(f), the stronger the RPV coupling the smaller the cross-section. In other terms, this signal is somehow complementary to the RPV ones discussed so far and requires a different discussion of the decay dynamics, given the additional dependence on the chargino mass. Hence, although this signature may well induce visible events in the end, we do not pursue further its study here.

4.6 The SM irreducible background

It is clear that the dominant SM irreducible background to RPV signals of the type discussed in the previous sections arises from associated production of a Z boson and a fermionic pair, with the gauge boson decaying into two further fermions:

$$\gamma\gamma \to Z\ell^\pm\ell^\mp \quad \text{or} \quad Zq\bar{q} \tag{13}$$

with

$$Z \to \ell'^{\pm}\ell'^{\mp} \;\; \text{or} \;\; Z \to q'\bar{q}' \,. \tag{14}$$

Only in the case of four-quark final states one has to deal with $W^{\pm}$ mediated production:

$$\gamma\gamma \to W^{\pm} q\bar{q}' \tag{15}$$

with

$$W^{\pm} \to q''\bar{q}''' \,. \tag{16}$$

However, notice that, with the exception of the $s\bar{s}s\bar{s}$ signature, only Cabibbo-Kobayashi-Maskawa (CKM) suppressed channels can contribute in (15)–(16), as we assume a fully efficient b quark tagging (via a displaced vertex) to be available at future LCs (*i.e.*, $\epsilon_b = 100\%$). This is precisely what occurs in the case of $s\bar{s}b\bar{b}$ final states whereas $W^{\pm}$ mediated SM backgrounds cannot contribute to $b\bar{b}b\bar{b}$ final states under the assumption of perfect b quark tagging.

The SM background cross-sections, after the cuts listed in eq. (10), are given in Table 4. A common feature to all rates is that they are basically independent of the polarisation state of the initial particles.

The Z mediated noise is in general at manageable level, as it is comparable in magnitude to the signal rates displayed in Figures 2–7, at least for rather light sneutrino masses. Only the case $s\bar{s}s\bar{s}$ seems disfavoured. This is easily explained by the fact that in the SM background rates a summation over u, d, s and c quark flavours is implied, whereas in the signal only s quarks contribute (recall that we assume only one λ' coupling at a time to be non-zero and notice that it is generally not possible to distinguish different light quark flavours[5]).

The enormous rates corresponding to the $W^{\pm}$ mediated background in the case of the $s\bar{s}s\bar{s}$ signature should not be surprising. In fact, in this background process, we also have included the contribution from intermediate production of vector boson pairs, *i.e.*, $\gamma\gamma \to W^{\pm}W^{\mp} \to W^{\pm}q\bar{q}'$[6], which is resonant in the decay $W^{\mp} \to q\bar{q}'$, hence intrinsically of order $1/\mathcal{O}(g_W^2)$ bigger in comparison to the case of $\gamma\gamma \to q\bar{q}$ contributions (followed by a vector boson bremsstrahlung), the all process further benefiting from relatively larger γW^+W^- and $W^{\pm}q\bar{q}'$ couplings, with respect to the $Zq\bar{q}$ ones. The same phenomenon occurs in the case of the $s\bar{s}b\bar{b}$ signature too, although here there is a compensating effect induced by the CKM suppression entering the $W^{\pm}$ coupling to fermion pairs, one of which is a b quark, as previously intimated.

[5] In fact, c quark vertex (anti-)tagging could be exploited too to reduce the contamination from the background, although to a lesser extent than in the case of a b flavour, because of the shorter lifetime of the latter in comparison. To avoid entering into unnecessary technicalities, we do not consider here such a possibility.

[6] We assume instead that charged Higgs mediated processes are negligible, because of the small Yukawa couplings involved (recall that we ignore top final states).

	$e^+e^-e^+e^-$	$\mu^+\mu^-\tau^+\tau^{-*}$	$\tau^+\tau^-\tau^+\tau^-$	$s\bar{s}s\bar{s}$	$s\bar{s}b\bar{b}^*$	$b\bar{b}b\bar{b}$
$\sigma(+-)$	1.53	2.89	1.35	30.44 40942.05	9.22 20.37	0.25
$\sigma(++)$	1.39	2.67	1.27	28.36 44979.58	8.63 22.53	0.24
$\sigma(00)$	1.47	2.79	1.32	29.54 41956.32	8.97 20.96	0.25
$\sqrt{s_{e^+e^-}} = 500$ GeV						
$\sigma(+-)$	1.12	2.16	1.04	23.94 52835.72	7.32 27.39	0.21
$\sigma(++)$	1.01	1.96	0.95	22.02 53003.61	6.73 26.78	0.19
$\sigma(00)$	1.07	2.07	1.00	23.12 54150.51	7.06 28.04	0.20
$\sqrt{s_{e^+e^-}} = 1$ TeV						
*Other c.c.'s are free from SM background						

Table 4: Cross sections in femtobarns for processes of the type (13)–(14) [upper rows] and (15)–(16) [lower rows], for the three beam polarisation configurations in Table 3, after the cuts in (10). Notice that, for both backgrounds, a sum over all non-b states is performed in the case of signatures involving s quarks.

One may attempt to reduce this contribution by removing events for which the invariant mass of the quark pair produced in association with the $W^\pm$ boson, $M_{q\bar{q}'}$, is close to M_W. As an exercise, we have imposed $|M_{q\bar{q}'} - M_W| > 5$ and 10 GeV in the generation of final states of the type (15) (alongside the usual cuts in energy and polar angle), and verified that the loss of background events is typically of just one order of magnitude, about a factor of 10 and 20, respectively, for the two cuts (somewhat smaller at 1 TeV than at 500 GeV). A much larger window in mass should be exploited to reject the unwanted $\gamma\gamma \to W^\pm W^\mp$ contributions, but this would be at the cost of a non-negligible loss of signal where the latter is largest (for $M_{\tilde{\nu}} \sim 100$ GeV), so that it would be not useful in the end. Indeed, we believe that only the $s\bar{s}b\bar{b}$ background can reasonably be brought under control without losing the bulk of the signal, not the $s\bar{s}s\bar{s}$ one.

If one then applies a similar cut on the decay products of the gauge vectors in (14)–(16), *i.e.*, $|M_{q'\bar{q}'} - M_Z| > 5(10)$ GeV and $|M_{q''\bar{q}'''} - M_W| > 5(10)$ GeV, similar background reductions as

above (10 and 20, respectively) can be seen. (These numbers are hardly spoiled by the combinatorics involved.) Hence, apart from the case of the $s\bar{s}s\bar{s}$ signature, which is swamped by the SM noise, for sneutrino masses in the ranges, say, 100 GeV $< M_{\tilde{\nu}} <$ 200 GeV for leptonic final states (provided μ is positive) and 100 GeV $< M_{\tilde{\nu}} <$ 300 GeV for hadronic ones (possibly, 400 GeV at higher collider energies), the other signals should comfortably be observable above the SM backgrounds considered here. For a typical 300 fb^{-1} of annual integrated luminosity, one may collect between several tens (at the upper ends of the mass interval above) and several hundreds (at the lower ends) of sneutrino events, for each extracted signature and independently of the polarisation state of the incoming electrons, positrons and laser photons. The effect of the mass cuts described above on the signal is marginal, as we have restricted our study to the case $M_\nu \gg M_V$, with $V = Z, W^\pm$, and since the sneutrino width is rather small, well below the GeV threshold. Besides, the fermions produced in association with the sneutrino yield a mass invariant distribution that is rather flat in the vicinity of the gauge boson masses (similarly, for all other two-particle masses that one can compute from the full four-body final states).

As a bonus, some leptonic signatures which are flavour changing, such as $\mu^+\mu^+\tau^-\tau^-$ and $\mu^-\mu^-\tau^+\tau^+$, would come practically free from SM background. The same may not be said for the corresponding hadronic cases, $ss\bar{b}\bar{b}$ and $\bar{s}\bar{s}bb$, unless the jet charge can be measured. This might be possible in the case of b quark tagging via its semi-leptonic decays, though the efficiency in this case is naturally of order 10% per tagged lepton flavour, as this is the size of the corresponding BR.

We have not simulated here any QCD background induced by $\gamma\gamma \to q\bar{q}g(\to q'\bar{q}')$ and $\gamma\gamma \to q\bar{q}g(\to gg)$ events, both yielding four-jet final states. In fact, we expect their contribution to be negligible. On the one hand, none of the di-jet invariant masses that can be formed there will have a tendency to concentrate around $M_{\tilde{\nu}}$ (rather, they will tend to diverge logarithmically as the invariant mass goes to zero). On the other hand, the two viable hadronic signatures considered here contain b quarks in the final state, so that the relevant QCD sample is naturally smaller in comparison to the complete one. Moreover, it should be recalled the smaller EM charge of b quarks with respect to the average one of the full QCD sample as well as the fact that the $g \to b\bar{b}$ splitting is kinematically mass suppressed. In the end, of the two viable hadronic signals, the $b\bar{b}b\bar{b}$ final state might well be the easiest one to extract from the QCD noise.

5 Conclusions

Although a full Monte Carlo simulation, including all signals and backgrounds that we have discussed and in presence of both hadronisation and detector effects, should eventually be performed in order to put on firmer ground the results presented here, it is clear that the latter seem rather

promising at present.

In practice, if RPV couplings of the type λ_{311}, λ_{323}, λ'_{323} or λ'_{333} are close to their current exclusion bounds, over sizable regions of the MSSM parameter space (particularly, for positive μ values), several four-fermion signatures induced by a sneutrino, with a mass up to 200 GeV at $\sqrt{s_{e^+e^-}} = 500$ GeV and 300–400 GeV at $\sqrt{s_{e^+e^-}} = 1$ TeV, produced in association with a fermion pair and decaying itself into a second pair, can be accessed at future LCs, with the photons produced via back-scattering against the primary electrons and positrons. The typical annual rate should be of several ten to hundred events, depending on the actual sneutrino mass and final state considered. If a high, but not unrealistic, degree of polarisation of both laser photons and leptonic beams can be achieved, this can be exploited to push the discovery reach in sneutrino mass even beyond the mentioned $M_{\tilde{\nu}}$ values, as the combination in which the electron and positron helicities have the same sign and opposite to the one of the laser photons yields, with increasing sneutrino mass, signal rates consistently and significantly above those induced in the other cases (including that of unpolarised beams), up to a factor of 4 or so larger in some instances. At the same time, typical SM backgrounds have been shown to be fairly insensitive to the polarisation state of the incoming particles. However, a sizable increase in luminosity (or run time) should also be considered alongside beam polarisation in order to cover this mass regime, as the RPV cross sections fall rather steeply with increasing sneutrino mass. Finally, it is not clear that beam polarisation will at all help for the lower mass intervals mentioned above, where the dependence of the signal rates on the helicity configuration of the incoming particles is very different from one channel to another.

6 Acknowledgements

We thank Abdesselam Arhrib for discussions. The work of DKG is supported by the National Science Council of Taiwan under the grant NSC 90-2811-M-002-054 and from the Ministry of Education Academic Excellence Project 89-N-FA01-1-4-3 of Taiwan.

References

[1] K. Abe *et al.*, [The ACFA Linear Collider Working Group], hep-ph/0109166 and references therein; T. Abe *et al.*, [The American Linear Collider Working Group], hep-ex/0106055; hep-ex/0106056; hep-ex/0106057 and hep-ex/0106058 and references therein; J.A. Aguilar-Saavedra *et al.*, [The ECFA/DESY LC Physics Working Group], preprint SLAC-REPRINT-2001-002, DESY-01-011, DESY-2001-011, DESY-01-011C, DESY-2001-

011C, DESY-TESLA-2001-23, DESY-TESLA-FEL-2001-05, ECFA-2001-209, March 2001, hep-ph/0106315; G. Guignard (editor), [The CLIC Study Team], preprint CERN-2000-008.

[2] I. Ginzburg , G. Kotkin, V. Serbo and V. Telnov, *Nucl. Instrum. Meth.* **A 205**, 47 (1983); *ibidem* **A 219**, 5 (1984); V. Telnov, *Nucl. Instrum. Meth.* **A 294**, 72 (1990).

[3] V. Telnov, hep-ex/0010033 and references therein.

[4] F. Cuypers, G.J. van Oldenborgh and R. Ruckl, *Nucl. Phys.* **B409**, 144 (1993).

[5] S. Berge, M. Klasen and Y. Umeda, *Phys. Rev.* D **63**, 35003 (2001); A. Datta and D. Choudhury, *Nucl. Phys.* **B592**, 35 (2001); T. Mayer and H. Fraas, *Nucl. Instrum. Meth.* **A 472**, 165 (2001); D. Gorbunov, V. Ilyin and V. Telnov, *Nucl. Instrum. Meth.* **A 472**, 171 (2001); D.M. Asner, J.B. Gronberg and J.F. Gunion, hep-ph/0110320 and references therein.

[6] D. E. Groom *et al.*, [Particle Data Group], *Eur. Phys. J.* **C15**, 1 (2000).

[7] P. Fayet, *Phys. Lett.* **B69**, 489 (1977); G. Farrar and P. Fayet, *Phys. Lett.* **B76**, 575 (1978); N. Sakai and T. Yanagida, *Nucl. Phys.* **B197**, 533 (1982); C. Aulakh and R. Mohapatra, *Phys. Lett.* **B119**, 136 (1983).

[8] S. Weinberg, *Phys. Rev.* D **26**, 287 (1982).

[9] L.J. Hall and M. Suzuki, *Nucl. Phys.* **B231**, 419 (1984); R. Barbieri and A. Masiero, *Nucl. Phys.* **B267**, 679 (1986); V. Barger, G. F. Giudice and T. Han, *Phys. Rev.* D **40**, 2987 (1989); R. Godbole, P. Roy and X. Tata, *Nucl. Phys.* **B401**, 67 (1993); G. Bhattacharyya, J.R. Ellis and K. Sridhar, *Mod. Phys. Lett.* **A10**, 1583 (1995); G. Bhattacharyya, D. Choudhury and K. Sridhar, *Phys. Lett.* **B355**, 193 (1995); D. Choudhury and S. Raychaudhury, *Phys. Lett.* **B401**, 54 (1997); D.K. Ghosh, S. Raychaudhuri and K. Sridhar, *Phys. Lett.* **B396**, 177 (1997); K. Huitu, J. Maalampi, M. Raidal and A. Santamaria, *Phys. Lett.* **B430**, 355 (1998); G. Moreau, '*Phenomenological study of the interactions violating the R-parity symmetry in the supersymmetric theories*', Ph.D. Thesis, hep-ph/0012156 and references therein.

[10] M. Chaichian, K. Huitu, S. Roy and Z.H. Yu, *Phys. Lett.* **B518**, 261 (2001).

[11] H. Murayama, I. Watanabe and K. Hagiwara, HELAS: HELicity Amplitude Subroutines for Feynman Diagram Evaluations, *KEK Report* 91–11, January 1992.

[12] T. Stelzer and W.F. Long, *Comp. Phys. Comm.* **81**, 357 (1994).

[13] G.P. Lepage, *Jour. Comp. Phys.* **27**, 192 (1978).

[14] L.J. Hall and M. Suzuki in Ref. [9]; I-H. Lee, *Phys. Lett.* **B138**, 121 (1984); *Nucl. Phys.* **B246**, 120 (1984); S. Dawson, *Nucl. Phys.* **B261**, 297 (1985); F. de Campos, M.A. Garcia-Jareno, A.S. Joshipura, J. Rosiek and J.W.F. Valle, *Nucl. Phys.* **B451**, 3 (1995); M. Nowakowski and A. Pilaftsis, *Nucl. Phys.* **B461**, 19 (1996); R. Hempfling, *Nucl. Phys.* **B478**, 3 (1996); S. Roy and B. Mukhopadhyaya, *Phys. Rev.* D **55**, 7020 (1997); M. Hirsch, M.A. Díaz, W. Porod, J.C. Romao and J.W.F. Valle, *Phys. Rev.* D **62**, 3008 (2000).

[15] S. Berge, M. Klasen and Y. Umeda, in Ref. [5].

[16] See, *e.g.*: B.C. Allanach, A. Dedes and H.K. Dreiner, *Phys. Rev.* D **60**, 075014 (1999) and references therein.

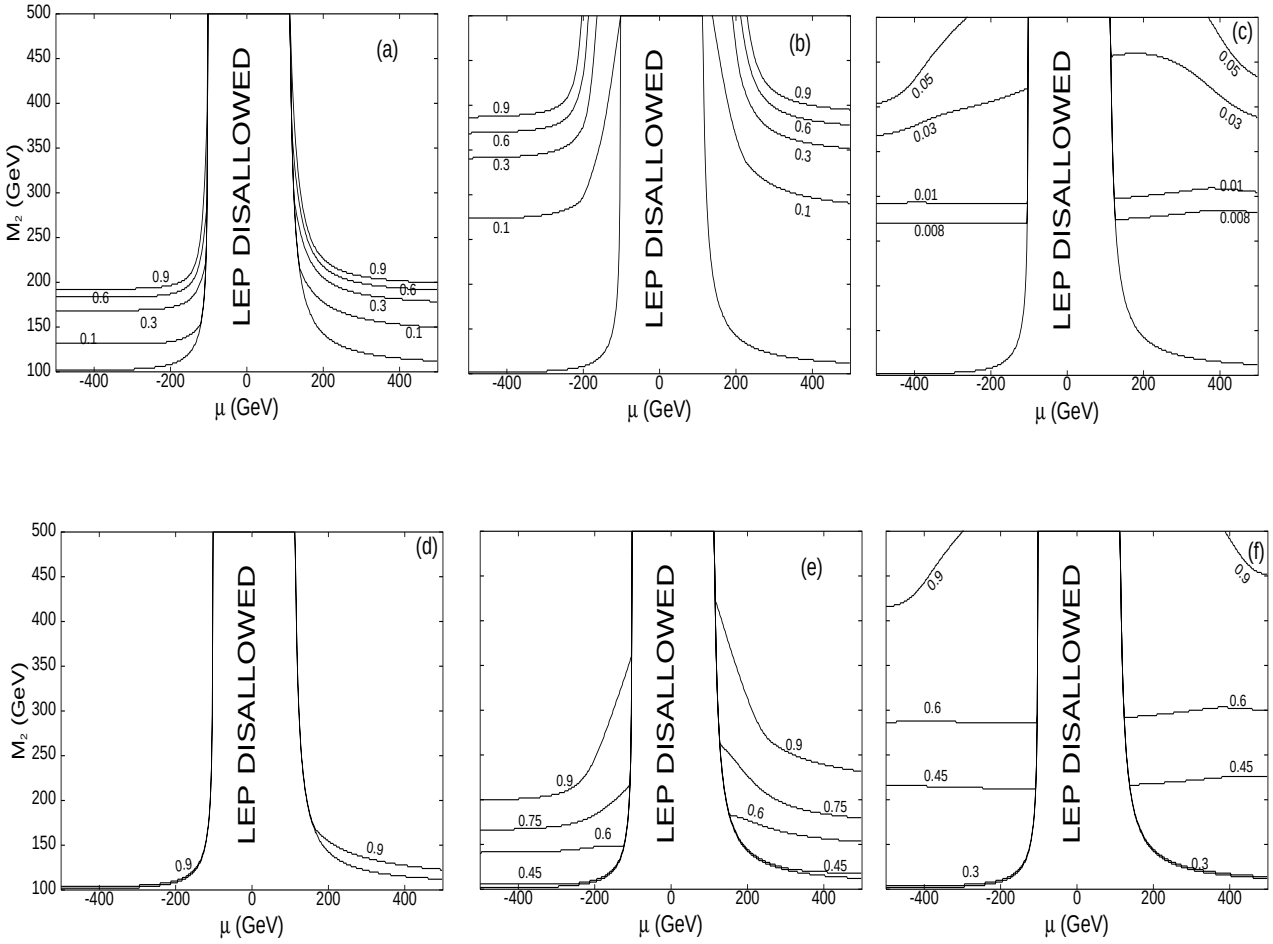

Figure 1: Constant BR contours of the decay $\tilde{\nu}_\tau \to e^+e^-$ for three values of sneutrino masses: 100 GeV (a), 200 GeV (b) and 400 GeV (c). Figures (d)–(f) represents contours of constant BR($\tilde{\nu}_\tau \to b\bar{b}$), again for a 100, 200 and 400 GeV sneutrino mass, respectively. The relevant L-violating couplings are here: $\lambda_{311} = 0.062$ for (a)–(c) and $\lambda'_{333} = 0.45$ for (d)–(f). We have fixed $\tan\beta = 5$.

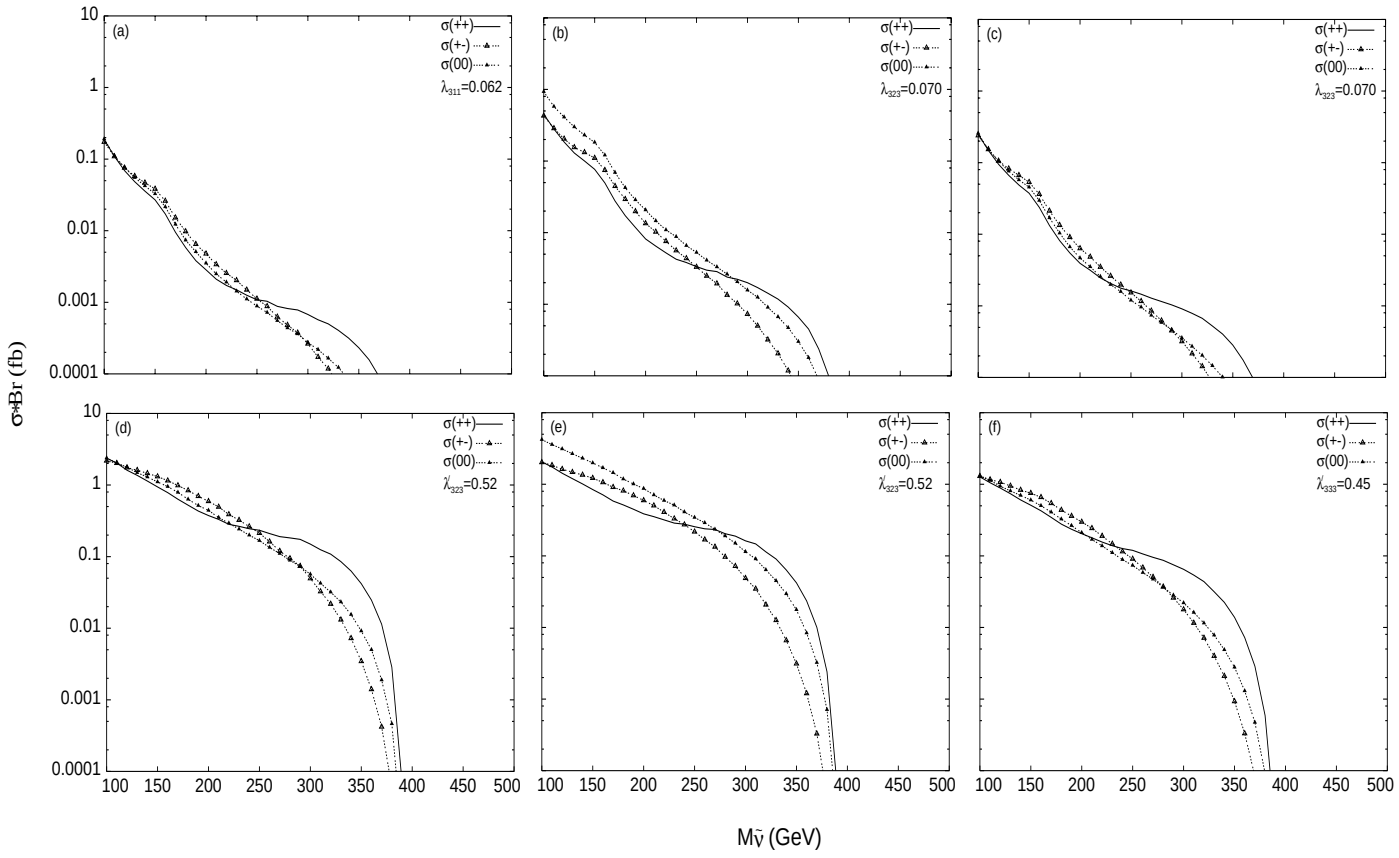

Figure 2: Variation of $\sigma(\gamma\gamma \to \tilde{\nu}_i f_j \bar{f}_k) * \mathrm{BR}(\tilde{\nu}_i \to f_j \bar{f}_k)$ at $\sqrt{s_{e^+e^-}} = 500$ GeV with the sneutrino mass, for fixed values of the relevant λ_{ijk} and λ'_{ijk} couplings. The MSSM parameters are $\mu = -400$ GeV, $M_2 = 150$ GeV and $\tan\beta = 5$ (set A). Figures (a)–(f) correspond to $e^+e^-e^+e^-$, $\mu^+\mu^-\tau^+\tau^-$ (including all c.c.'s), $\tau^+\tau^-\tau^+\tau^-$, $s\bar{s}s\bar{s}$, $s\bar{s}b\bar{b}$ (including all c.c.'s) and $b\bar{b}b\bar{b}$ final states, respectively. See Table 3 for the definition of (un)polarised cross-sections.

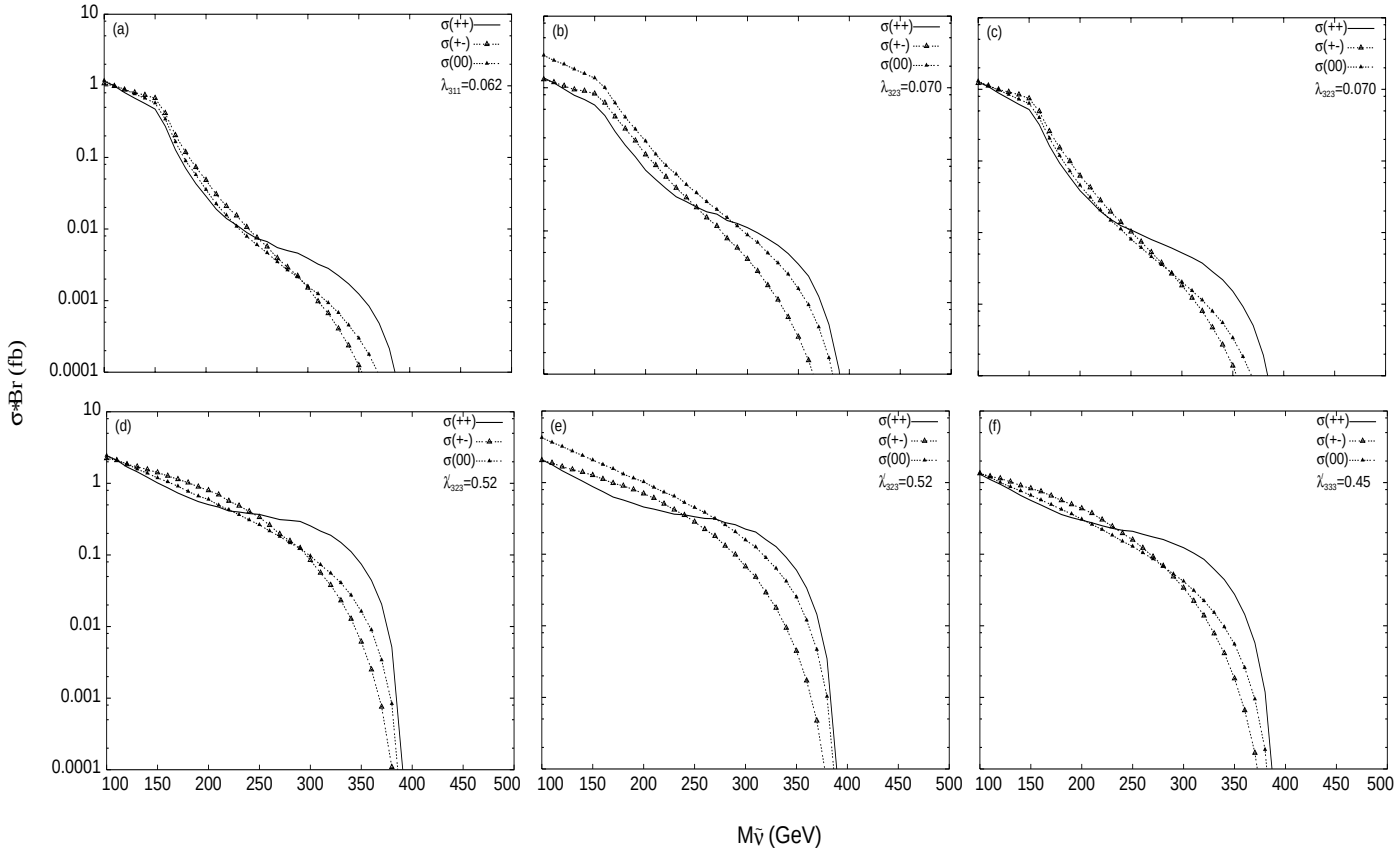

Figure 3: Variation of $\sigma(\gamma\gamma \to \tilde{\nu}_i f_j \bar{f}_k) * \mathrm{BR}(\tilde{\nu}_i \to f_j \bar{f}_k)$ at $\sqrt{s_{e^+e^-}} = 500$ GeV with the sneutrino mass, for fixed values of the relevant λ_{ijk} and λ'_{ijk} couplings. The MSSM parameters are $\mu =$ 200 GeV, $M_2 = 350$ GeV and $\tan\beta = 40$ (set B). Final state flavours and other parameters are as in Figure 2. Similarly, for the conventions of the (un)polarised cross sections.

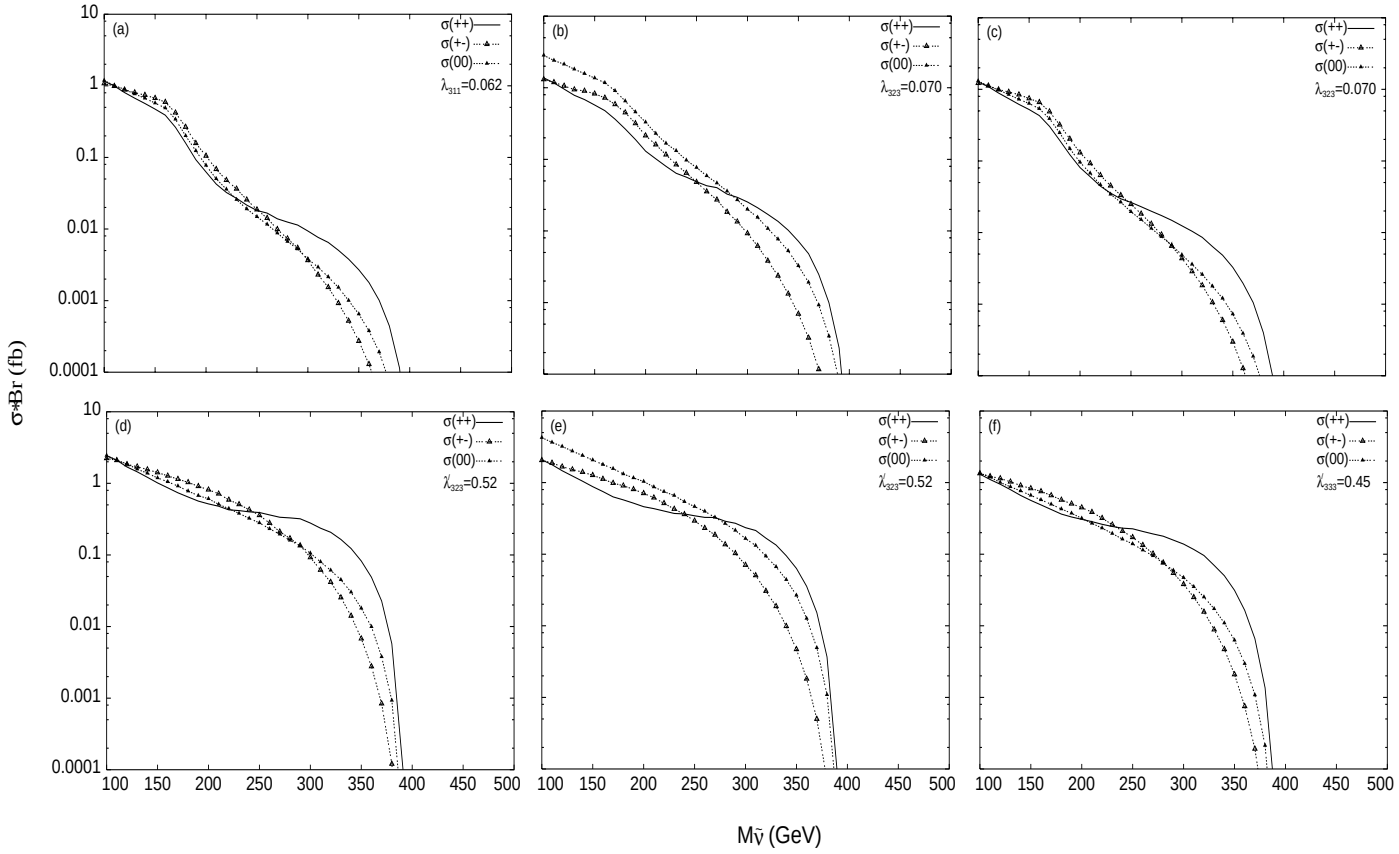

Figure 4: Variation of $\sigma(\gamma\gamma \to \tilde{\nu}_i f_j \bar{f}_k) * \mathrm{BR}(\tilde{\nu}_i \to f_j \bar{f}_k)$ at $\sqrt{s_{e^+e^-}} = 500$ GeV with the sneutrino mass, for fixed values of the relevant λ_{ijk} and λ'_{ijk} couplings. The MSSM parameters are $\mu = 175$ GeV, $M_2 = 500$ GeV and $\tan\beta = 40$ (set C). Final state flavours and other parameters are as in Figure 2. Similarly, for the conventions of the (un)polarised cross sections.

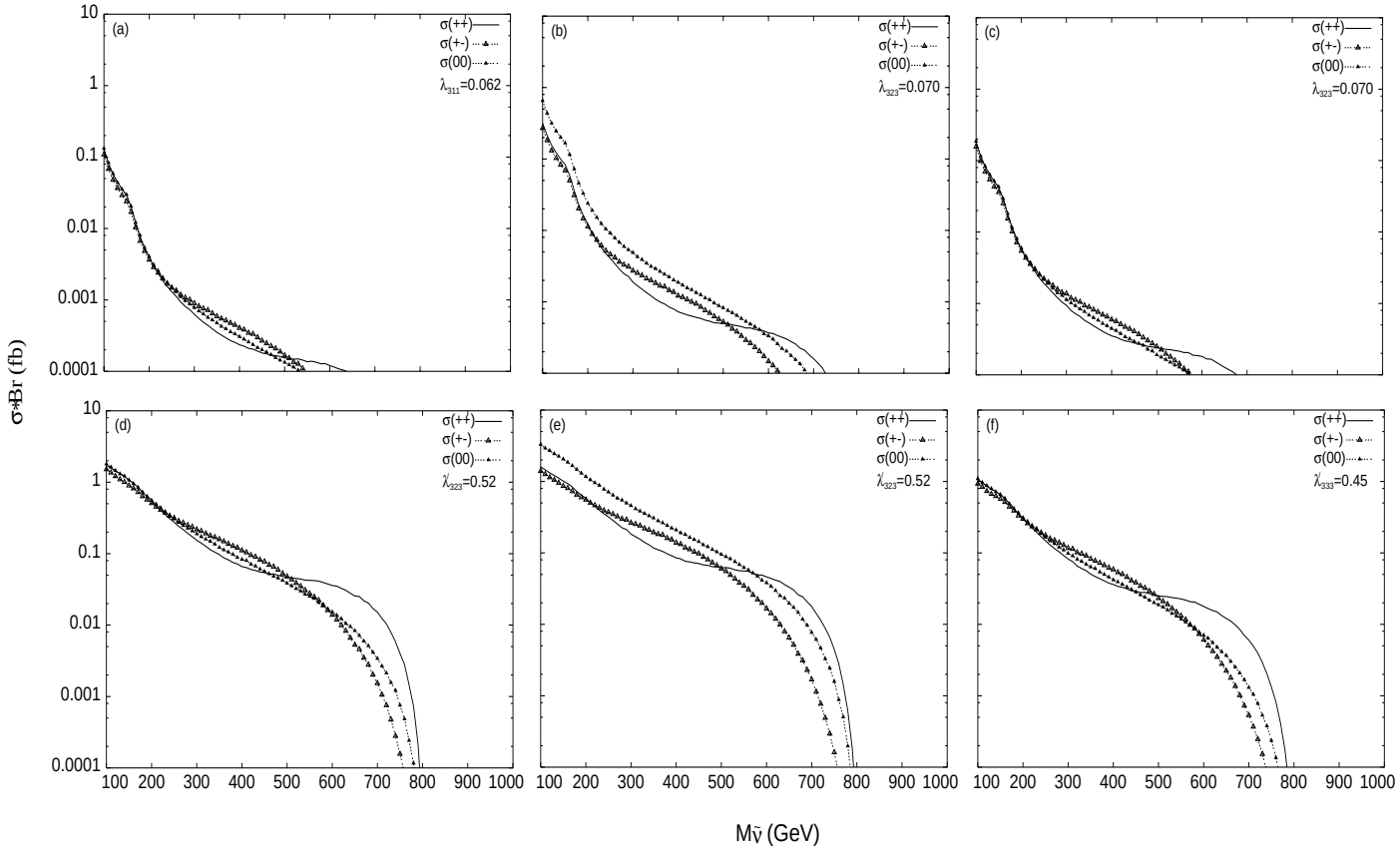

Figure 5: Variation of $\sigma(\gamma\gamma \to \tilde{\nu}_i f_j \bar{f}_k) * \mathrm{BR}(\tilde{\nu}_i \to f_j \bar{f}_k)$ at $\sqrt{s_{e^+e^-}} = 1$ TeV with the sneutrino mass, for fixed values of the relevant λ_{ijk} and λ'_{ijk} couplings. The MSSM parameters are $\mu = -400$ GeV, $M_2 = 150$ GeV and $\tan\beta = 5$ (set A). Final state flavours and other parameters are as in Figure 2. Similarly, for the conventions of the (un)polarised cross sections.

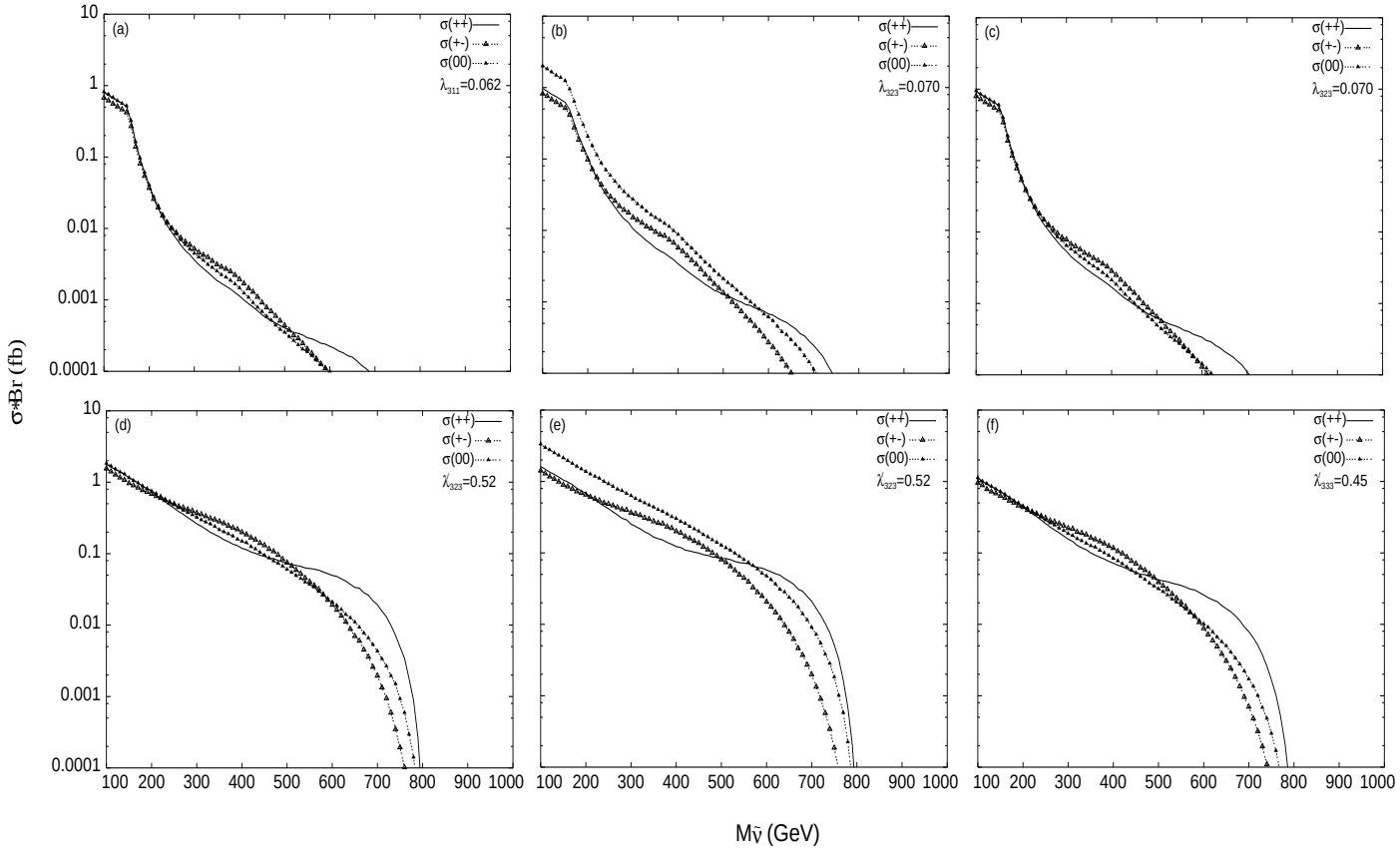

Figure 6: Variation of $\sigma(\gamma\gamma \to \tilde{\nu}_i f_j \bar{f}_k) * \mathrm{BR}(\tilde{\nu}_i \to f_j \bar{f}_k)$ at $\sqrt{s_{e^+e^-}} = 1$ TeV with the sneutrino mass, for fixed values of the relevant λ_{ijk} and λ'_{ijk} couplings. The MSSM parameters are $\mu =$ 200 GeV, $M_2 = 350$ GeV and $\tan\beta = 40$ (set B). Final state flavours and other parameters are as in Figure 2. Similarly, for the conventions of the (un)polarised cross sections.

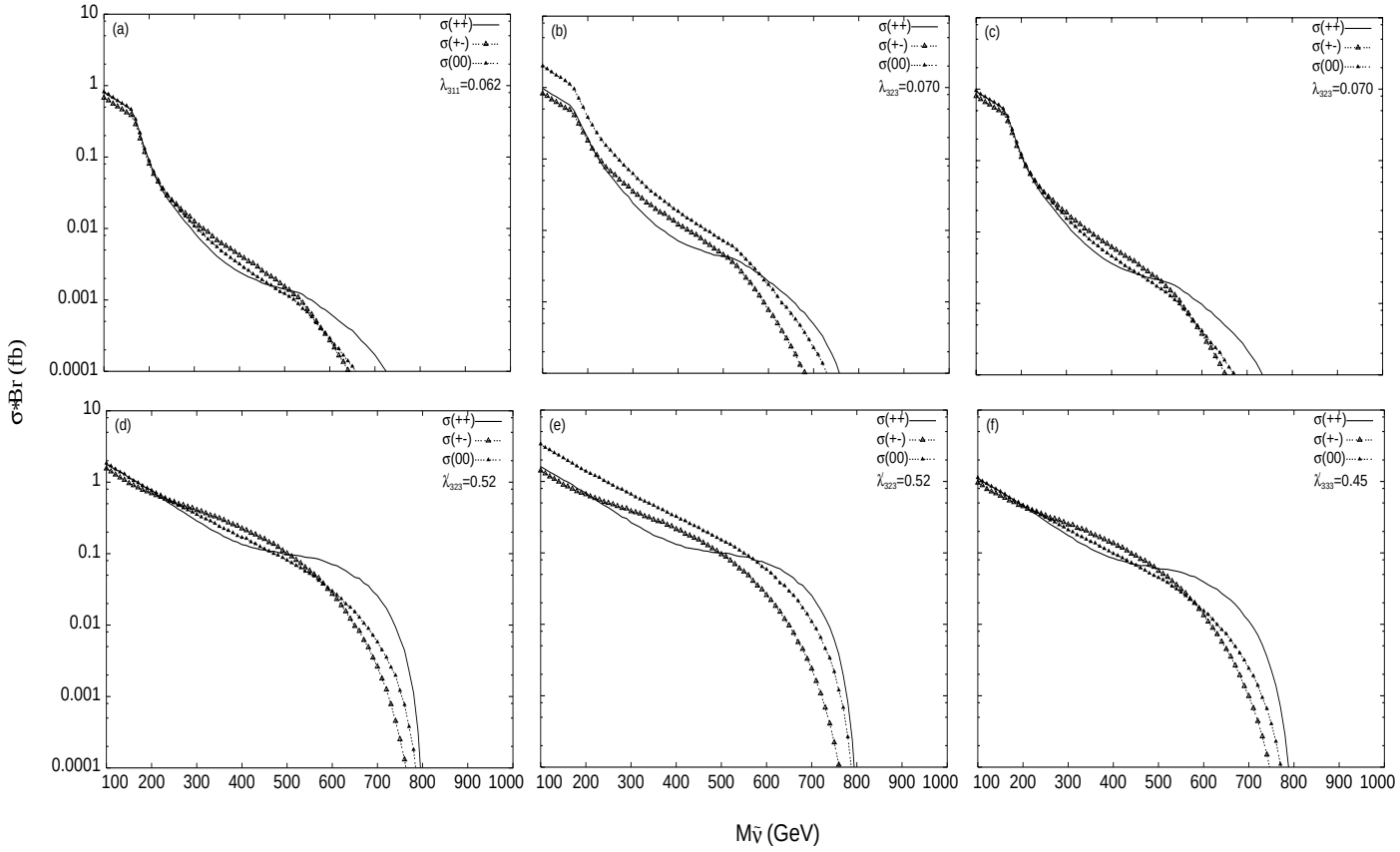

Figure 7: Variation of $\sigma(\gamma\gamma \to \tilde{\nu}_i f_j \bar{f}_k) * \mathrm{BR}(\tilde{\nu}_i \to f_j \bar{f}_k)$ at $\sqrt{s_{e^+e^-}} = 1$ TeV with the sneutrino mass, for fixed values of the relevant λ_{ijk} and λ'_{ijk} couplings. The MSSM parameters are $\mu =$ 175 GeV, $M_2 = 500$ GeV and $\tan\beta = 40$ (set C). Final state flavours and other parameters are as in Figure 2. Similarly, for the conventions of the (un)polarised cross sections.

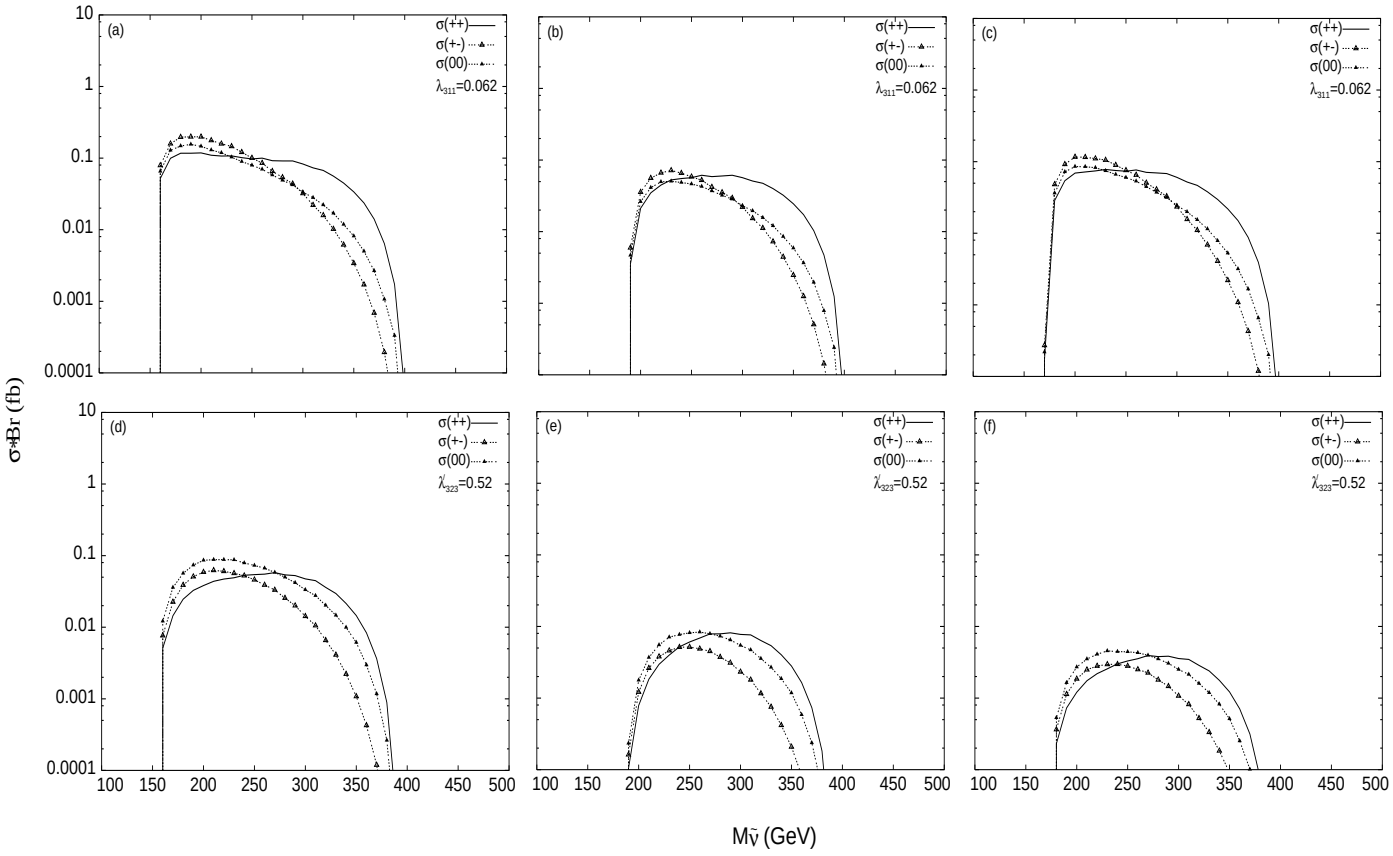

Figure 8: Variation of $\sigma(\gamma\gamma \to \tilde{\nu}_i f_j \bar{f}_k) * \mathrm{BR}(\tilde{\nu}_i \to \ell^- \tilde{\chi}_1^+)$ at $\sqrt{s_{e^+e^-}} = 500$ GeV with the sneutrino mass, for fixed values of the relevant λ_{ijk} and λ'_{ijk} couplings. Figures (a)–(c) correspond to $\sigma(\gamma\gamma \to \tilde{\nu}_\tau e^+ e^-) * \mathrm{BR}(\tilde{\nu}_\tau \to \tau^- \tilde{\chi}_1^+)$ with $\lambda_{311} = 0.062$. Figures (d)–(f) correspond to $\sigma(\gamma\gamma \to \tilde{\nu}_\tau s\bar{b}) * \mathrm{BR}(\tilde{\nu}_\tau \to \tau^- \tilde{\chi}_1^+)$ with $\lambda'_{323} = 0.52$. Labels (a,d), (b,e) and (c,f) correspond to the three different sets A, B and C of MSSM parameters, respectively. Beam polarization conventions are the same as in the previous Figures.